

Reentrant Localization in Quasiperiodic Thue-Morse Chain

Taylan Yıldız* and B. Tanatar†

Department of Physics, Bilkent University, 06800 Ankara, Türkiye

(Dated: December 23, 2025)

We investigate localization and reentrance in a dimerized Su-Schrieffer-Heeger (SSH) tight-binding chain whose on-site energies are given by a quasiperiodic cosine masked by a deterministic Thue-Morse sequence. Working with non-interacting, spinless fermions, we solve the model via exact diagonalization on large Fibonacci sizes and diagnose phases using inverse/normalized participation ratios and the correlation fractal dimension. We identify boundaries separating extended, multi-fractal (mixed), and localized regimes by constructing a phase diagram in the plane of modulation strength and dimerization ratio. As the quasiperiodic amplitude is increased, the system exhibits reentrant behavior, localizing, partially re-delocalizing into a multifractal regime, and re-localizing, verified via two-size crossings of band-averaged observables and finite-size scaling. We demonstrate that tuning the modulation strength, the SSH dimerization, or the incommensurability parameter provides control over the critical thresholds. Our results suggest a versatile, randomness-free platform for the deterministic control of transport, enabling switching between conducting, multifractal, and insulating states.

I. INTRODUCTION

Disorder and aperiodicity profoundly reshape wave propagation in low-dimensional systems. In one dimension, uncorrelated randomness generically localizes all single-particle states (Anderson localization)[1], while correlated quasiperiodic potentials, most famously the Aubry-André-Harper (AAH) model [2–4], produce sharply tunable metal-insulator transitions and rich critical regimes without true randomness. These quasiperiodic lattices have also been studied with different models to entangle localization properties [5–26], including many-body extensions characterized as many-body localization (MBL) [27–31]. These localization transitions have also been investigated in various experimental settings; AL observed in optics (localization of strongly scattered light became an early observation) [32], in photonic lattices [33, 34], in elastic waves [35] and in ultra cold atoms [36] whereas quasiperiodic localization also observed in optical lattices [37–39], in cold atoms [40] and in superconducting qubits [41]. Beyond these cases, recent work has uncovered a striking non-monotonic phenomenon: reentrant localization, where increasing the strength of the modulation can localize, then partially redelocalize, and finally relocalize eigenstates as parameters are varied. This behavior has been reported in several 1D quasiperiodic settings, including dimerized (SSH) chains and generalized AAH variants [42–53], and raises a basic question: which microscopic ingredients control the emergence and robustness of re-entrance?

In this paper, we address that question in a dimerized quasiperiodic chain with two sublattices per unit cell (SSH geometry [54]) whose on-site energies are modulated by an incommensurate cosine and masked by a

deterministic Thue-Morse (TM) sequence. The TM sequence is a paradigmatic aperiodic order: it is binary, perfectly balanced at large scales, and endowed with long-range substitutional correlations distinct from both periodic staggering and uncorrelated randomness [55–57]. This makes it an ideal test for separating the roles of global balance, determinism, and correlation structure in driving re-entrant behavior. The TM sequence has also been investigated in condensed matter physics using different models, as seen in [58–61].

First, we chart the localization landscape of this TM-masked SSH chain, identifying extended, critical (multifractal), and localized regions, and isolating reentrant parameter windows where states delocalize after an initial localization onset before ultimately relocating at stronger modulation. Second, we develop and apply finite-size scaling diagnostics that allow us to locate critical disorder strengths and extract critical exponents. Alongside standard markers, the inverse participation ratio (IPR), normalized participation ratio (NPR), and the correlation fractal dimension obtained via a box-counting procedure, we introduce a two-size crossing analysis of the order parameter over targeted spectral windows. The crossing function yields size-independent fixed points at criticality, providing precise estimates of the localization threshold and critical exponents.

In summary, the TM-masked SSH model provides an analytically transparent setting in which reentrant localization can be tracked with high resolution. By combining participation-based metrics, multifractal analysis, and crossing-function finite-size scaling on Fibonacci system sizes, we map out the phase structure, quantify critical behavior, and clarify the microscopic origin of re-entrance in a deterministic aperiodic environment. These results contribute to the growing picture that quasiperiodic and aperiodic order can host localization phenomena that are qualitatively distinct from both periodic crystals and fully random media, with potential implications for wave control in photonic, cold-atom, and mesoscopic

* taylan.yildiz@bilkent.edu.tr

† tanatar@fen.bilkent.edu.tr

platforms.

The remainder of this paper is organized as follows. In Sec. II, we introduce the Thue-Morse modulated quasiperiodic SSH Hamiltonian, specify the on-site potential, and summarize the numerical techniques and localization diagnostics, including fractal dimension, IPR, and NPR. In Sec. III we present our main results, which track the real-space and multifractal evolution of the eigenstates, construct a localization phase diagram with respect to hopping and disorder strengths, and analyze representative hopping values. We then identify the critical disorder strengths using a two-size crossing analysis and corroborate the results with a finite-size scaling analysis of the participation ratio. In Sec. IV we summarize our conclusions and discuss the physical origin of the reentrant localization. Appendix A provides a study of where the Thue-Morse sequence is replaced by a random (balanced and unbiased) binary sequence to test the role of the Thue-Morse sequence.

II. MODEL AND METHOD

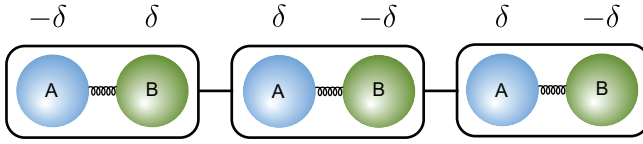


FIG. 1. Illustration of the model described with 3 unit cells and with length 6 Thue-Morse sequence

We consider a one-dimensional quasiperiodic chain with two sublattices in each cell. The tight-binding Hamiltonian follows as:

$$H = -J_1 \sum_{n=1}^N c_{n,\alpha}^\dagger c_{n,\beta} + h.c - J_2 \sum_{n=1}^N c_{n,\beta}^\dagger c_{n+1,\alpha} + h.c + \sum_{n=1}^N \epsilon_{n,\alpha} c_{n,\alpha}^\dagger c_{n,\alpha} + \epsilon_{n,\beta} c_{n,\beta}^\dagger c_{n,\beta} \quad (1)$$

This is an SSH Hamiltonian with N unit cells containing two sublattice sites α and β . $c_{n,\alpha}^\dagger$ ($c_{n,\alpha}$) and $c_{n,\beta}^\dagger$ ($c_{n,\beta}$) are creation (annihilation) operators for sublattice α and β . The intracell and intercell hopping strengths are denoted by J_1 and J_2 , respectively. Onsite energies for two sublattice $\epsilon_{n,\alpha}$ and $\epsilon_{n,\beta}$ read as:

$$\begin{aligned} \epsilon_{n,\alpha} &= (-1)^{S_{2n-1}} \delta \cos(2\pi\beta(2n-1) + \phi_1) \\ \epsilon_{n,\beta} &= (-1)^{S_{2n}} \delta \cos(2\pi\beta(2n) + \phi_2) \end{aligned} \quad (2)$$

where δ is the quasiperiodic potential strength, β is the irrational frequency, $\phi_{1,2}$ are the potential phases and S_n is the n th element of the Thue-Morse sequence:

$$S_0 = 0, \quad S_{2n} = S_n, \quad S_{2n+1} = 1 - S_n \quad (3)$$

The first few elements of the sequence read as 0110100110010110...

We choose $\beta = (\sqrt{5} - 1)/2$, inverse golden ratio for the irrational period of the potentials [2, 6, 22, 62]. We fix intra-cell hopping $J_1 = 1$ and also fix $\phi_{1,2} = 0$ without loss of generality since we are using long enough chains in our study. To analyze the localization transition in our model, we rely on multi-fractal analysis [63], mainly the correlation dimension D_2 . We define the fractal dimension of the i th eigenstate $D_f^{(i)}$ as:

$$D_f^{(i)} = - \lim_{L \rightarrow \infty} \frac{1}{f-1} \frac{\ln P_f^{(i)}}{\ln L} \quad (4)$$

where $L = 2N$ is the total system size and

$$P_f^{(i)} = \sum_{n=1}^L |\psi_n^{(i)}|^{2f} \quad (5)$$

is the f th moment. If we let $f = 2$ in the generalized fractal dimension, we get the correlation dimension D_2 .

$$D_2^{(i)} = - \lim_{L \rightarrow \infty} \frac{\ln P_2^{(i)}}{\ln L} \quad (6)$$

where we call P_2 as the inverse participation ratio (IPR) [64, 65].

$$\text{IPR}^{(i)} = \sum_{n=1}^L |\psi_n^{(i)}|^4 \quad (7)$$

We also analyze the localization transition by using the normalized participation ratio (NPR)

$$\text{NPR}^{(i)} = \left(L \sum_{n=1}^L |\psi_n^{(i)}|^4 \right)^{-1} = \frac{\text{PR}^{(i)}}{L} \quad (8)$$

where PR stands for participation ratio.

III. RESULTS

In our numerical calculations, we use Fibonacci-sized systems up to $N = 6765$ and set hopping dimerization $J_2 = 0.7$ (we scale all energies by J_1).

A. Fractal Dimension Analysis

In Fig. 2 we find that the wavefunction exhibits a non-monotonic evolution of the mid-band eigenstate with δ : extended at $\delta = 0$, sharply localized near $\delta = 0.6$, partially delocalized (multifractal) around $\delta \approx 1.1$, and localized again by $\delta = 3.0$. We will investigate this localized \rightarrow delocalized \rightarrow localized sequence and the multifractal spectrum with the correlation fractal dimension.

We employ the box-counting method to estimate the correlation dimension D_2 [66–69]. We select a family of

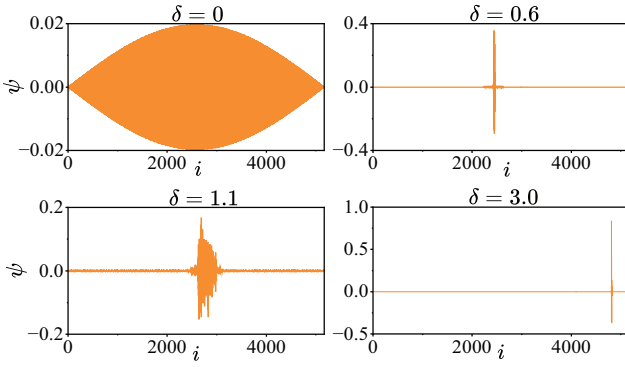


FIG. 2. Real-space profiles of the middle eigenstate ψ_i (eigen-index $m/L = 0.5$) for four potential strengths $\delta = 0, 0.6, 1.1$, and 3.0 . Parameters: system size $N = 2584$, $J_2 = 0.7$.

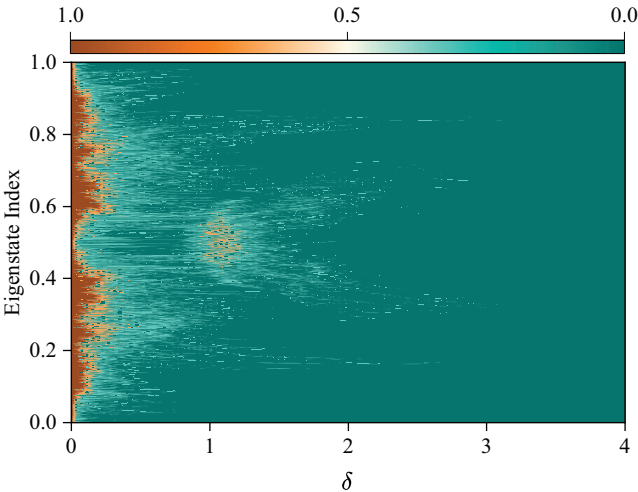


FIG. 3. Density plot of fractal dimension D_2 with respect to eigenstate index with the system size 1597 and with 20 different box sizes

box scales $\{l_j\}$. For each l_j , partition boxes L/l_j of length l_j . In a box k ;

$$\mu_k(l_j) = \sum_{i=(k-1)l_j+1}^{kl_j} p_i \quad (9)$$

where $p_i = |\psi_i|^2$ is the probability of the i th eigenstate, then $\mu_k(l_j)$ is the total probability of the wavefunction in that box. From the sum of probabilities of the different boxes, the second moment (IPR) reads as

$$\text{IPR}(l_j) = P_2(l_j) = \sum_{k=1}^{L/l_j} \{\mu_k(l_j)\}^2 \quad (10)$$

It is known that IPR scales as L^{-D_2} with respect to the size of the system. Then, by performing a regression analysis on $\ln \text{IPR}(l_j)$ and $\ln l_j$ we can find the correlation dimension of the system.

In Fig. 3 we show the density plot of the correlation fractal dimension D_2 for every eigenstate as a function of disorder strength δ . The color scale runs from $D_2 = 0$ (green, fully localized) to $D_2 = 1$ (orange, fully extended). We see that for very small values of δ nearly all states have $D_2 \approx 1$, indicating Bloch-like delocalization similar to the clean SSH chain. Slightly increasing the potential strength, we see that a tongue of reduced D_2 (green) appears first in the mid-spectrum, showing that these states become neither fully extended nor localized, but develop nontrivial power-law scaling of their inverse participation ratios. near $\delta \approx 0.8$, immediately beyond the first critical window, there is a slight increase in D_2 (lightening), signaling a transient delocalization before the final localization transition. At large disorder, the entire spectrum collapses to $D_2 \approx 0$, as every eigenstate becomes exponentially localized by the strong quasiperiodic Thue–Morse potential.

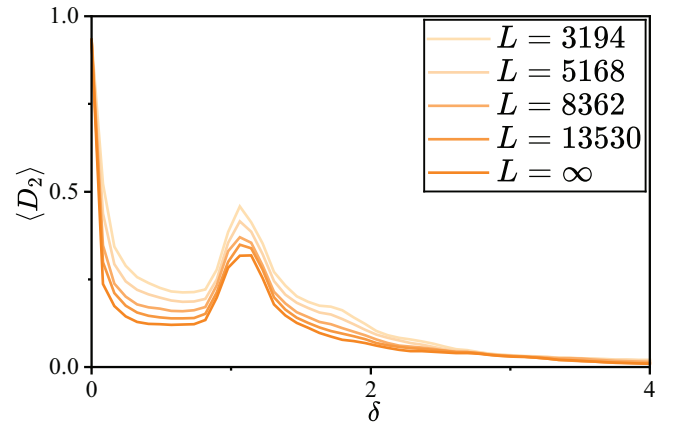


FIG. 4. Averaged fractal dimension D_2 over the middle of the spectrum with respect to δ for $N = 1597, 2584, 4181, 6765$ and extrapolated result for $N \rightarrow \infty$.

Figure 4 plots the spectrum-averaged fractal dimension $\langle D_2 \rangle$ of the central 300–900 states (depending on N) versus disorder strength δ , for four Fibonacci sizes and an extrapolated $N \rightarrow \infty$ curve. All finite- N curves display a pronounced dip–peak (“re-entrant”) feature near $\delta \approx 0.7$ – 1.2 before decaying to zero at strong disorder. Notably, as N increases, the height of the re-entrant bump diminishes and its maximum shifts slightly to lower δ , and the $N \rightarrow \infty$ estimate (green) lies below every finite- N trace in that window. This demonstrates that while multifractal reentrance is a robust phenomenon, its amplitude and precise location are renormalized in the thermodynamic limit.

B. IPR and NPR ANALYSIS

Alongside the fractal dimension, we will analyze the spectrum with individual finite-sized IPR and NPR for robustness. For the IPR and NPR analysis, we will use

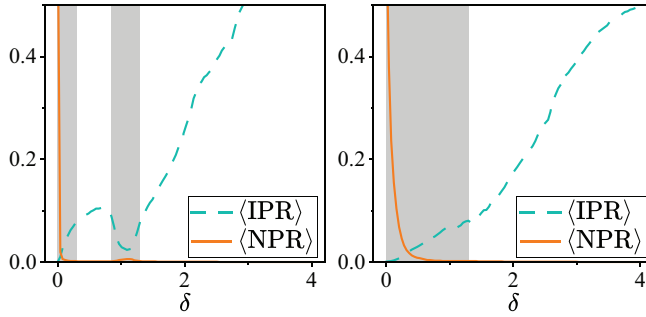


FIG. 5. Average IPR and NPR with respect to potential strength δ for states in the middle of the spectra and for system size $L = 13530$, shaded regions correspond to critical phases. (a) for $J_2 = 0.7$ (b) for $J_2 = 1.2$

the band-averaged IPR and NPR to get the information about the desired window of eigenstates.

$$\langle \text{IPR} \rangle = \frac{1}{M} \sum_{i \in M} \text{IPR}^{(i)}, \quad \langle \text{NPR} \rangle = \frac{1}{M} \sum_{i \in M} \text{NPR}^{(i)} \quad (11)$$

In Fig. 5(a), we plot the averaged IPR and NPR for the

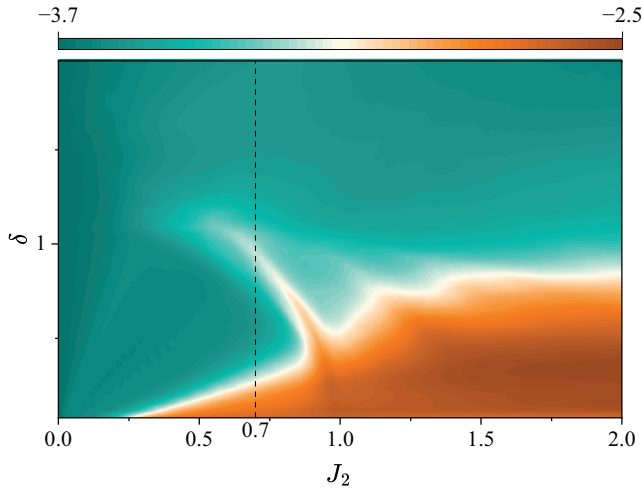


FIG. 6. Phase map of the composite metric η in the (J_2, δ) plane. The translucent boxes and the inset highlight reentrant regions, and the vertical dotted lines mark representative J_2 cuts discussed in the text. Color represents the values of η

middle of the spectrum as a function of disorder strength δ for $J_2 = 0.7$. At very small δ , the spectrum is in critical phase (shaded region). We see that with a slight increase in δ , all states become localized ($\text{NPR} \rightarrow 0$). As δ is further increased in the critical window (shaded region), these localized states begin to delocalize, indicating that the system has momentarily “re-entered” a multifractal phase. Pushing δ even higher, the NPR suddenly falls again, indicating a second localization transition. In strong agreement with the Fig. 4 correlation dimension analysis. Panel (b) uses a different dimeriza-

tion $J_2 = 1.2$. This time we do not observe dip–peak–dip sequence in NPR. This suggests that the reentrance behavior is specific to certain dimerization.

Now, to observe the effect of other dimerization ratios we will build a phase map in the (δ, J) plane using the composite ratio [8, 42]

$$\eta \equiv \log_{10}(\langle \text{IPR} \rangle \times \langle \text{NPR} \rangle) \quad (12)$$

Where we have $\eta < -\log_{10} L$ when the spectrum is almost entirely localized or extended, and we have $-2 \lesssim \eta \lesssim -1$ when the extended and localized states coexist (multifractal state). We clearly see the reentrant feature in the phase diagram Fig. 6 between $J_2 = 0$ and $J_2 = 1$. We also observe that there are no other dimerization windows for the reentrance, which only happens when $J_2 < 1$.

To monitor the evolution of the individual eigenstates more clearly with $J_2 = 0.7$, we compare localization indicators with the density of states (DOS) at four representative quasiperiodic strengths, $\delta = 0, 0.1, 0.6, 1.1$, and 3.0 in Figs. 7 and 8. For weak disorder ($\delta = 0.1$) most eigenstates are extended (small IPR, sizable NPR), consistent with the DOS concentrated in two clean minibands. At $\delta = 0.6$ the first localization onset appears in the middle of the spectrum: NPR is suppressed and IPR spikes precisely within the shaded DOS windows, identifying localized subbands (mobility-gap regions).

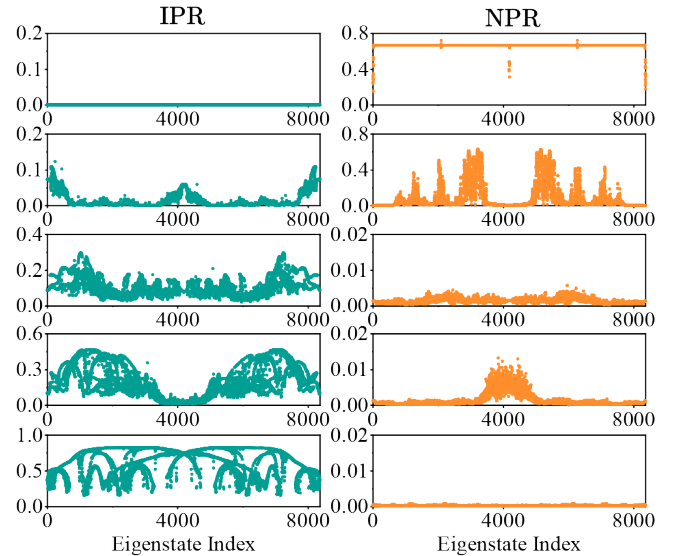


FIG. 7. Left column: inverse participation ratio (IPR, green) and Right column: normalized participation ratio (NPR, orange) vs. eigenstate index at five disorder strengths (top to bottom): $\delta = 0, 0.1, 0.6, 1.1, 3.0$. Here $N = 4181, J_2 = 0.7$

A re-entrant behavior emerges near $\delta \approx 1.1$: after the initial localization around $\delta \sim 0.6$, the mid-band NPR partially recovers and IPR dips, indicating transient re-delocalization before localization strengthens again at larger δ . For strong quasiperiodicity ($\delta = 3.0$) NPR is nearly zero and IPR is large over most of the spectrum,

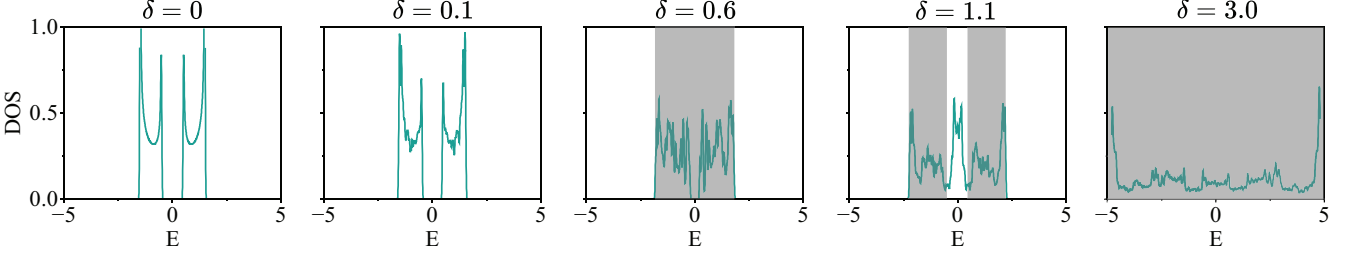


FIG. 8. Normalized density of states (DOS) vs. energy for five disorder strengths (left to right): $\delta = 0, 0.1, 0.6, 1.1, 3.0$ and for $N = 4181$, with shaded bands indicating the localized states.

matching the broadly shaded DOS regions and signaling global localization. Thus, the shaded DOS intervals mark energies where eigenstates are localized, while unshaded regions correspond to more extended or critical states.

C. Critical State Analysis

In this section, we try to identify the transition points by doing a critical state analysis. First, we define the order parameter of the system. The finite-size order parameter is the square root of the band-averaged NPR,

$$\sigma(\delta; L) \equiv \sqrt{\langle \text{NPR} \rangle} = \left[\frac{1}{M} \sum_{m \in \mathcal{S}} \text{NPR}^{(m)} \right]^{1/2} \quad (13)$$

where \mathcal{S} is a narrow window of eigenstates. At the transition point, observables display a power law behaviour indicated by [70]

$$\sigma \sim (-\varepsilon)^\beta, \quad \text{PR} \sim \varepsilon^{-\gamma}, \quad \xi \sim |\varepsilon|^{-\nu}. \quad (14)$$

where $\varepsilon = (\delta - \delta_c)/\delta_c$, δ_c is the critical disorder strength. We have β , γ , and ν are the order parameter, participation ratio, and localization length exponent, respectively. Then we have

$$\text{PR}(\delta, L) \sim L^{\gamma/\nu} G(\varepsilon L^{1/\nu}), \quad (15)$$

$$\sigma^2(\delta, L) \sim L^{\gamma/\nu-1} G(\varepsilon L^{1/\nu}). \quad (16)$$

where F and G are scaling functions. For any pair (L, L') we define two-size crossing function as

$$R[L, L'](\delta) \equiv \frac{\ln(\sigma^2(\delta, L)/\sigma^2(\delta, L'))}{\ln(L/L')} + 1 \quad (17)$$

From the scaling form, all curves $R[L, L'](\delta)$ intersect at a common δ_c and their height at the crossing equals γ/ν (size-independent fixed point). This provides a precise estimator of δ_c and γ/ν .

In Fig. 9, we plot the two size crossing functions for three size pairs $(1974, 5168)$, $(3194, 8362)$, $(5168, 13530)$. For the first localization transition, we used the band edge of the eigenstates to get $R[L, L'](\delta)$ since we know

from our previous analysis that the first localization happens at the edge states (Fig. 7). In Fig. 9(a), we identify the point where all three curves cross, the critical disorder strength $\delta_c = 0.0205$ corresponds to the first localization transition, and the critical exponent $\gamma/\nu = 0.04$, which is the ordinate of the common crossing point. For the transition to the multifractal state, we switch to use the middle band of the eigenstates and identify the critical values as $\delta_c = 0.7552$ and $\gamma/\nu = 0.025$ in Fig. 9(b). The third graph Fig. 9(c) represents the second localization transition (reentrance) again we identify the common crossing point of the curves, which corresponds to the values $\delta_c = 1.0488$ and $\gamma/\nu = 0.03$.

In addition, we try to confirm the critical values obtained by the two-size crossing function from the scaling relation of the participation ratio PR with the system size L .

$$\text{PR} \sim L^{\gamma/\nu} \quad (18)$$

Figure 10 shows $\ln \overline{\text{PR}}$ versus $\ln L$ at the critical disorders extracted from the two-size-crossing analysis, together with linear fits of the form $\ln \overline{\text{PR}} = a + (\gamma/\nu) \ln L$. The slope of each fit gives the estimate of γ/ν .

For the first transition at $\delta_c = 0.0205$, we obtain $\gamma/\nu = 0.0423 \pm 0.008$ Fig. 10(a), consistent with the crossing result. For the second transition at $\delta_c = 0.7552$, the fit yields $\gamma/\nu = 0.0244 \pm 0.004$ Fig. 10(b), again in good agreement. For the third transition at $\delta_c = 1.04885$, we find $\gamma/\nu = 0.0236 \pm 0.006$ from the $\ln \overline{\text{PR}} - \ln L$ fit, whereas the crossing height gives $\gamma/\nu \simeq 0.030$ Fig. 10(c). This mild tension is plausibly due to finite-size drift and window sensitivity (different subbands entering the mid-band average for different L); using only the largest sizes and/or narrowing the m/L window should reduce the discrepancy. Overall, the small fitted slopes corroborate that $\overline{\text{PR}}$ is nearly scale independent at the critical points.

IV. CONCLUSION

Our study demonstrates that a one-dimensional quasiperiodic lattice with hopping dimerization and Thue-Morse modulation exhibits reentrant localization. We explored the transitions and the multifractal nature

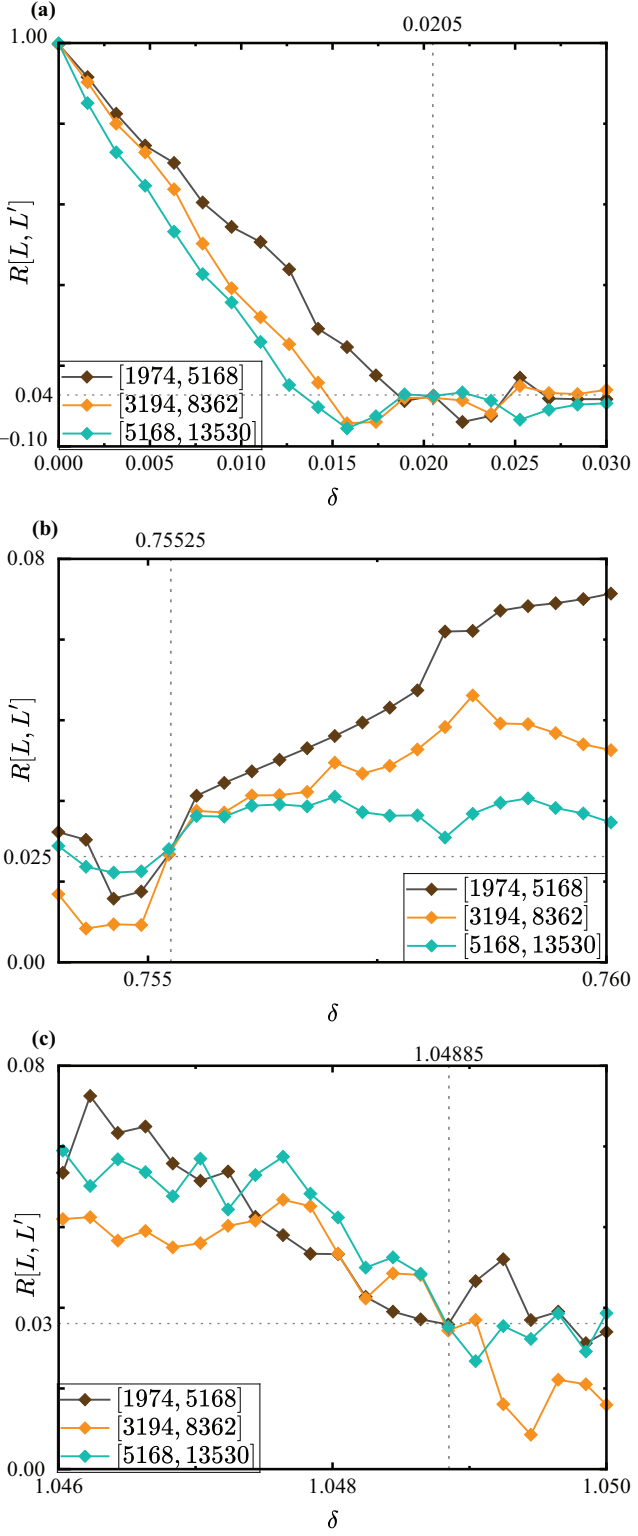


FIG. 9. Two-size crossing analysis, curves are shown for the equal-ratio pairs (1974, 5168), (3194, 8362), and (5168, 13530). (a) average taken over the window edge $m/L \in [0, 0.05]$, (b) and (c): averages over the mid-band window $m/L \in [0.475, 0.525]$. Vertical dashed lines mark the common-crossing points. Horizontal dashed lines mark γ/ν

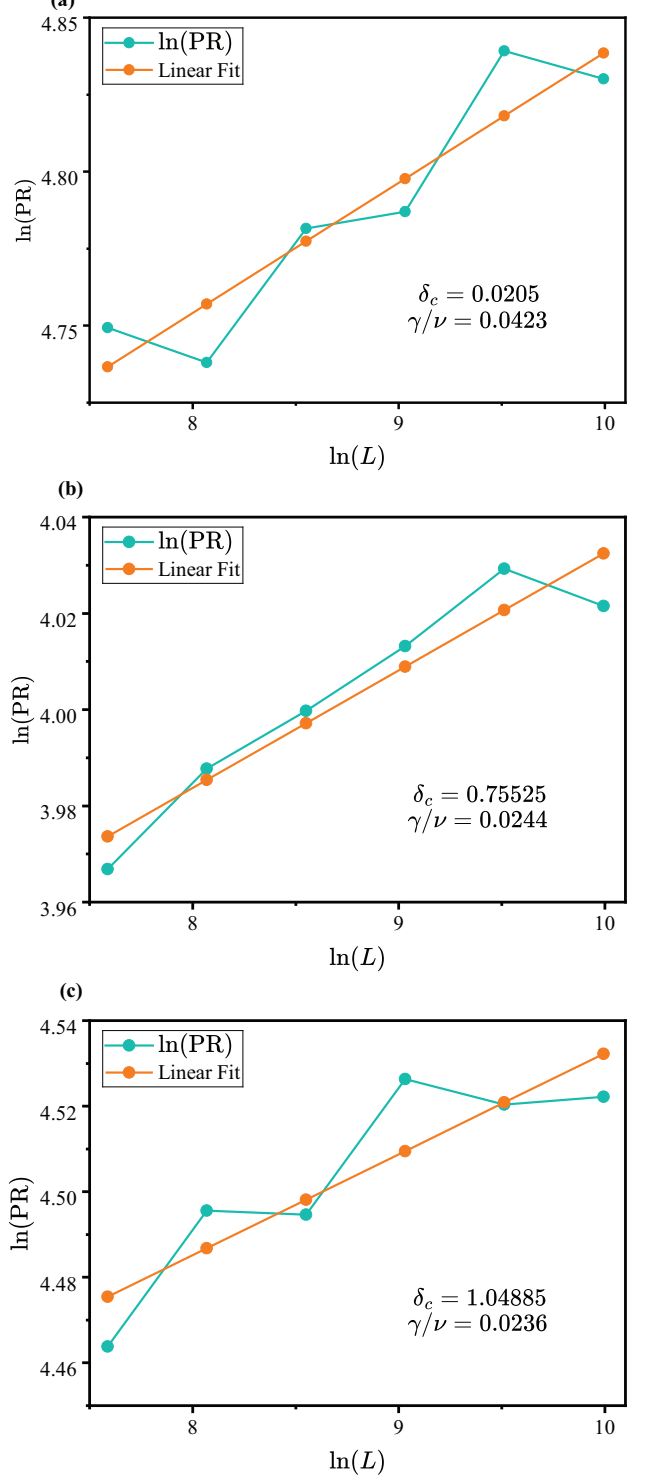


FIG. 10. Finite-size scaling of the participation ratio at the three critical disorder strengths. In each panel, we plot the band-averaged $\ln \overline{PR}$ versus $\ln L$ and fit to the linear form $\ln \overline{PR} = a + (\gamma/\nu) \ln L$; the slope yields γ/ν . (a) Window edge $m/L \in [0, 0.05]$ (b) and (c) Mid-band window $m/L \in [0.475, 0.525]$. The small slopes indicate that \overline{PR} is nearly scale-independent at criticality, almost consistent with the small crossing heights obtained from the two-size analysis.

of the eigenstates by performing exact diagonalization on large Fibonacci lattice sizes and characterizing the states via the IPR, NPR, and the fractal dimension obtained from a box-counting analysis. For suitable hopping dimerization, we observe that the system undergoes a second localization transition, signalling a reentrance from localized to extended (or critical) and back to localized behavior. We complemented these findings with a careful finite-size analysis of the corresponding order parameters to extract the critical disorder strengths. Finally, we showed that the reentrance is absent when the Thue–Morse sequence is replaced by a random binary sequence, indicating that this phenomenon relies on the deterministic correlations of the Thue–Morse modulation. Overall, our results show that reentrance is not restricted to simple staggered potentials and provide a new platform to examine localization transitions in quasiperiodic models.

ACKNOWLEDGMENTS

This work was supported in part by the Turkish Academy of Sciences (TUBA) under Grant No. AD-2025.

Appendix A: Checking Reentrance with Random Binary Sequences

The reentrant delocalized pocket reported in the main text for the Thue–Morse (TM) modulation could, in principle, be an artifact of the sitewise parity balance (equal number of 0s and 1s) rather than the deterministic aperiodic correlations of the TM sequence. To disentangle these possibilities we repeat the phase–diagram calculation after replacing TM by two ensembles of random binary sequences: (i) an unbiased i.i.d. Bernoulli ensemble and (ii) a balanced random ensemble that preserves the global 50/50 parity but destroys all correlations.

Model and ensembles

We keep the Hamiltonian exactly as in the main text, with open boundary conditions (OBC) and dimerized hoppings $J_1 = 1$ and J_2 . The on–site energies are

$$\varepsilon_m = (-1)^{S_m} \delta \cos(2\pi\beta m + \phi), \quad (1)$$

where $\beta = (\sqrt{5} - 1)/2$ is the inverse golden ratio and $\phi = 0$. The binary sequence $S_m \in \{0, 1\}$ is drawn as:

- **Unbiased random:** $S_m \stackrel{\text{i.i.d.}}{\sim} \text{Bernoulli}(1/2)$.
- **Balanced random:** exactly $L/2$ ones and $L - L/2$ zeros, uniformly shuffled.

Thus the second ensemble shares the same global parity balance as TM but no longer has its long–range substitution correlations.

The color variable is the same as in the main text,

$$\eta \equiv \log_{10}(\langle \text{IPR} \rangle \times \langle \text{NPR} \rangle) \quad (2)$$

with eigenstate averages taken over a fixed index window around the band center, $m/L \in [0.475, 0.525]$ (we also verified edge windows $m/L \in [0, 0.05]$ as a control). For each grid point (J_2, δ) we average η over 10 independent sequence realizations.

Phase maps and comparison

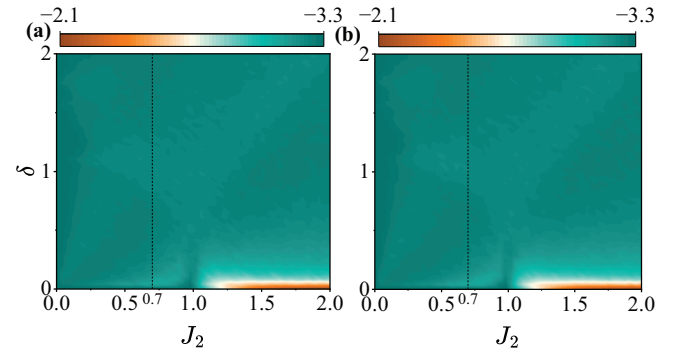


FIG. 11. Phase diagrams of η in the (J_2, δ) plane for random binary sequences. (a) Unbiased i.i.d. Bernoulli sequence. (b) Balanced random sequence with an equal number of 0's and 1's. Averages are taken over the mid-band window $m/L \in [0.475, 0.525]$, $L = 1974$ and averaged over 10 sequence realizations. The vertical dashed line marks $J_2 = 0.7$, the cut discussed in the main text.

Figures 11(a) and 11(b) display the phase diagrams for the unbiased and balanced ensembles, respectively. Relative to the TM case main text, Fig. 6. The sharp cusp and the reentrant “tongue” are strongly suppressed once correlations are removed. The unbiased ensemble shows a mostly monotonic crossover from the extended to localized regime (green) almost with no critical regions (orange) as δ increases. Enforcing only the global 50/50 balance (balanced random) does not change the behavior of unbiased ensemble and does not restore the reentrant feature.

We confirmed these statements by examining average IPR and NPR at fixed J_2 in Fig. 12 (dashed lines in the figures): IPR and NPR varies smoothly with δ for both random ensembles and shows no characteristic of reentrance.

Conclusion

Randomizing the binary modulation (either fully or under a global balance constraint) removes the reentrant

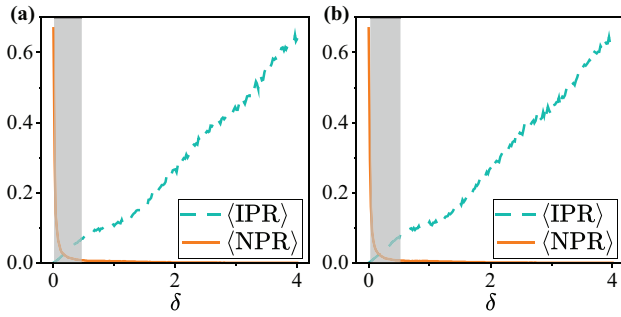


FIG. 12. Average IPR and NPR with respect to potential strength δ for states in the middle of the spectra and for system size $L = 1974$, shaded regions correspond to critical phases. (a) for an unbiased i.i.d Bernoulli sequence (b) balanced random sequence with an equal number of 0's and 1's.

[1] P. W. Anderson, Absence of Diffusion in Certain Random Lattices, *Phys. Rev.* **109**, 1492 (1958).

[2] S. Aubry and G. André, Analyticity breaking and Anderson localization in incommensurate lattices, *Ann. Israel Phys. Soc.* **3**, 18 (1980).

[3] P. G. Harper, Single band motion of conduction electrons in a uniform magnetic field, *Proc. Phys. Soc. Sect. A* **68**, 874 (1955).

[4] D. R. Hofstadter, Energy levels and wave functions of Bloch electrons in rational and irrational magnetic fields, *Phys. Rev. B* **14**, 2239 (1976).

[5] J. Biddle, B. Wang, D. Priour Jr, and S. Das Sarma, Localization in one-dimensional incommensurate lattices beyond the Aubry-André model, *Phys. Rev. A* **80**, 021603 (2009).

[6] C. Soukoulis and E. Economou, Localization in One-Dimensional Lattices in the Presence of Incommensurate Potentials, *Phys. Rev. Lett.* **48**, 1043 (1982).

[7] M. Johansson and R. Riklund, Self-dual model for one-dimensional incommensurate crystals including next-nearest-neighbor hopping, and its relation to the Hofstadter model, *Phys. Rev. B* **43**, 13468 (1991).

[8] X. Li and S. Das Sarma, Mobility edge and intermediate phase in one-dimensional incommensurate lattice potentials, *Phys. Rev. B* **101**, 064203 (2020).

[9] M. Rossignolo and L. Dell'Anna, Localization transitions and mobility edges in coupled Aubry-André chains, *Phys. Rev. B* **99**, 054211 (2019).

[10] X. Deng, S. Ray, S. Sinha, G. Shlyapnikov, and L. Santos, One-dimensional quasicrystals with power-law hopping, *Phys. Rev. Lett.* **123**, 025301 (2019).

[11] J. Biddle, D. Priour Jr, B. Wang, and S. Das Sarma, Localization in one-dimensional lattices with non-nearest-neighbor hopping: Generalized Anderson and Aubry-André models, *Phys. Rev. B* **83**, 075105 (2011).

[12] N. Roy and A. Sharma, Study of counterintuitive transport properties in the Aubry-André-Harper model via entanglement entropy and persistent current, *Phys. Rev. B* **100**, 195143 (2019).

[13] G. Domínguez-Castro and R. Paredes, The Aubry-André model as a hobbyhorse for understanding the localization phenomenon, *Eur. J. Phys.* **40**, 045403 (2019).

[14] J. Biddle and S. Das Sarma, Predicted Mobility Edges in One-Dimensional Incommensurate Optical Lattices: An Exactly Solvable Model of Anderson Localization, *Phys. Rev. Lett.* **104**, 070601 (2010).

[15] L. Gong, Y. Feng, and Y. Ding, Anderson localization in one-dimensional quasiperiodic lattice models with nearest-and next-nearest-neighbor hopping, *Phys. Lett. A* **381**, 588 (2017).

[16] N. Roy and A. Sharma, Fraction of delocalized eigenstates in the long-range Aubry-André-Harper model, *Phys. Rev. B* **103**, 075124 (2021).

[17] H. Yao, A. Khoudli, L. Bresque, and L. Sanchez-Palencia, Critical Behavior and Fractality in Shallow One-Dimensional Quasiperiodic Potentials, *Phys. Rev. Lett.* **123**, 070405 (2019).

[18] B. Hetényi and I. Balogh, Numerical study of the localization transition of aubry-andré type models, *Phys. Rev. B* **112**, 144203 (2025).

[19] C. Monthus, Multifractality in the generalized Aubry-André quasiperiodic localization model with power-law hoppings or power-law Fourier coefficients, *Fractals* **27**, 1950007 (2019).

[20] M. Gonçalves, B. Amorim, E. V. Castro, and P. Ribeiro, Critical phase dualities in 1D exactly solvable quasiperiodic models, *Phys. Rev. Lett.* **131**, 186303 (2023).

[21] S. Ganguly and S. K. Maiti, Electrical analogue of one-dimensional and quasi-one-dimensional Aubry-André-Harper lattices, *Sci. Reports* **13**, 13633 (2023).

[22] S. Y. Jitomirskaya, Metal-insulator transition for the almost Mathieu operator, *Ann. Math.* **150**, 1159 (1999).

[23] M. Wilkinson, Critical Properties of Electron Eigenstates in Incommensurate Systems, *Proc. R. Soc. Lond. A* **391**, 305 (1984).

[24] S. Roy, S. K. Maiti, and D. Laroze, Anomalous persistent current in a 1d dimerized ring with aperiodic site potential: Non-interacting and interacting cases, *Chin. J. Phys.* (2025).

[25] A. Szabó and U. Schneider, Mixed spectra and partially extended states in a two-dimensional quasiperiodic model, *Phys. Rev. B* **101**, 014205 (2020).

[26] C. W. Duncan, Critical states and anomalous mobility edges in two-dimensional diagonal quasicrystals, *Phys. Rev. B* **109**, 014210 (2024).

[27] S. Ray, M. Pandey, A. Ghosh, and S. Sinha, Localization of weakly interacting Bose gas in quasiperiodic potential, *New J. Phys.* **18**, 013013 (2015).

[28] D. Vu, K. Huang, X. Li, and S. Das Sarma, Fermionic many-body localization for random and quasiperiodic systems in the presence of short-and long-range interactions, *Phys. Rev. Lett.* **128**, 146601 (2022).

[29] S. Bera, H. Schomerus, F. Heidrich-Meisner, and J. H. Bardarson, Many-body localization characterized from a one-particle perspective, *Phys. Rev. Lett.* **115**, 046603 (2015).

[30] K. Huang, D. Vu, X. Li, and S. Das Sarma, Incommensurate many-body localization in the presence of long-range hopping and single-particle mobility edge, *Phys. Rev. B* **107**, 035129 (2023).

[31] A. V. M. Marino, M. A. Caracanhas, V. S. Bagnato, and B. Chakrabarti, Dynamical localization of interacting ultracold atoms in one-dimensional quasi-periodic potentials (2025), arXiv:2509.19421 [cond-mat.quant-gas].

[32] D. S. Wiersma, P. Bartolini, A. Lagendijk, and R. Righini, Localization of light in a disordered medium, *Nature* **390**, 671 (1997).

[33] T. Schwartz, G. Bartal, S. Fishman, and M. Segev, Transport and anderson localization in disordered two-dimensional photonic lattices, *Nature* **446**, 52 (2007).

[34] Y. Lahini, A. Avidan, F. Pozzi, M. Sorel, R. Morandotti, D. N. Christodoulides, and Y. Silberberg, Anderson localization and nonlinearity in one-dimensional disordered photonic lattices, *Phys. Rev. Lett.* **100**, 013906 (2008).

[35] H. Hu, A. Strybulevych, J. Page, S. E. Skipetrov, and B. A. van Tiggelen, Localization of ultrasound in a three-dimensional elastic network, *Nat. Phys.* **4**, 945 (2008).

[36] J. Billy, V. Josse, Z. Zuo, A. Bernard, B. Hambrecht, P. Lugan, D. Clément, L. Sanchez-Palencia, P. Bouyer, and A. Aspect, Direct observation of Anderson localization of matter waves in a controlled disorder, *Nature* **453**, 891 (2008).

[37] Y. Lahini, R. Pugatch, F. Pozzi, M. Sorel, R. Morandotti, N. Davidson, and Y. Silberberg, Observation of a localization transition in quasiperiodic photonic lattices, *Phys. Rev. Lett.* **103**, 013901 (2009).

[38] M. Schreiber, S. S. Hodgman, P. Bordia, H. P. Lüschen, M. H. Fischer, R. Vosk, E. Altman, U. Schneider, and I. Bloch, Observation of many-body localization of interacting fermions in a quasirandom optical lattice, *Science* **349**, 842 (2015).

[39] H. P. Lüschen, S. Scherg, T. Kohlert, M. Schreiber, P. Bordia, X. Li, S. Das Sarma, and I. Bloch, Single-particle mobility edge in a one-dimensional quasiperiodic optical lattice, *Phys. Rev. Lett.* **120**, 160404 (2018).

[40] G. Roati, C. D'Errico, L. Fallani, M. Fattori, C. Fort, M. Zaccanti, G. Modugno, M. Modugno, and M. Inguscio, Anderson localization of a non-interacting Bose-Einstein condensate, *Nature* **453**, 895 (2008).

[41] P. Roushan, C. Neill, J. Tangpanitanon, V. M. Bastidas, A. Megrant, R. Barends, Y. Chen, Z. Chen, B. Chiaro, A. Dunsworth, *et al.*, Spectroscopic signatures of localization with interacting photons in superconducting qubits, *Science* **358**, 1175 (2017).

[42] S. Roy, T. Mishra, B. Tanatar, and S. Basu, Reentrant Localization Transition in a Quasiperiodic Chain, *Phys. Rev. Lett.* **126**, 106803 (2021).

[43] A. Padhan, S. R. Padhi, and T. Mishra, Complete delocalization and reentrant topological transition in a non-Hermitian quasiperiodic lattice, *Phys. Rev. B* **109**, L020203 (2024).

[44] S. Ganguly, S. Sarkar, K. Mondal, and S. K. Maiti, Phenomenon of multiple reentrant localization in a double-stranded helix with transverse electric field, *Sci. Reports* **14**, 3059 (2024).

[45] A. Padhan, M. K. Giri, S. Mondal, and T. Mishra, Emergence of multiple localization transitions in a one-dimensional quasiperiodic lattice, *Phys. Rev. B* **105**, L220201 (2022).

[46] S. Roy, S. Chattopadhyay, T. Mishra, and S. Basu, Critical analysis of the reentrant localization transition in a one-dimensional dimerized quasiperiodic lattice, *Phys. Rev. B* **105**, 214203 (2022).

[47] C. Wu, J. Fan, G. Chen, and S. Jia, Non-Hermiticity-induced reentrant localization in a quasiperiodic lattice, *New J. Phys.* **23**, 123048 (2021).

[48] X.-P. Jiang, Y. Qiao, and J.-P. Cao, Mobility edges and reentrant localization in one-dimensional dimerized non-Hermitian quasiperiodic lattice, *Chin. Phys. B* **30**, 097202 (2021).

[49] H. Wang, X. Zheng, L. Xiao, S. Jia, J. Chen, and L. Zhang, Coexistence of reentrant localization and dynamical delocalization in a one-dimensional non-Hermitian quasiperiodic lattice, *Phys. Rev. B* **112**, 054202 (2025).

[50] R. Ghosh, M. Sarkar, and I. M. Khaymovich, Reentrant localization induced by short-range hopping in the fractal Rosenzweig-Porter model, *Phys. Rev. B* **111**, L220102 (2025).

[51] X.-M. Wang, S.-Z. Li, and Z. Li, Emergent topological re-entrant phase transition in a generalized quasiperiodic modulated Su-Schrieffer-Heeger model, *Phys. Rev. A* **111**, 022214 (2025).

[52] S. Ganguly, S. Chattopadhyay, K. Mondal, and S. K. Maiti, Critical analysis of multiple reentrant localization in an antiferromagnetic helix with transverse electric field: Hopping dimerization-free scenario, *SciPost Phys.* **8**, 012 (2025).

[53] P.-J. Chang, Q.-B. Zeng, J. Pi, D. Ruan, and G.-L. Long, Investigation of reentrant localization transition in one-dimensional quasi-periodic lattice with long-range hopping, *New J. Phys.* **27**, 053501 (2025).

[54] W.-P. Su, J. R. Schrieffer, and A. J. Heeger, Solitons in Polyacetylene, *Phys. Rev. Lett.* **42**, 1698 (1979).

[55] A. Thue, Über unendliche zeichenreihen, *Selsk. Skr. Mat. Nat. Kl.* **7**, 1 (1906).

[56] E. Prouhet, Mémoire sur quelques relations entre les puissances des nombres, *C.R. Acad. Sci. Paris* **33**, 1851 (1851).

[57] H. M. Morse, Recurrent geodesics on a surface of negative curvature, *Trans. Amer. Math. Soc.* **22**, 84 (1921).

[58] Z. Cheng, R. Savit, and R. Merlin, Structure and electronic properties of Thue-Morse lattices, *Phys. Rev. B* **37**, 4375 (1988).

[59] M. Kolář, M. Ali, and F. Nori, Generalized Thue-Morse chains and their physical properties, *Phys. Rev. B* **43**, 1034 (1991).

[60] L. Moretti and V. Mocella, Two-dimensional photonic aperiodic crystals based on Thue-Morse sequence, *Opt. Express* **15**, 15314 (2007).

- [61] C. Ryu, G. Oh, and M. Lee, Extended and critical wave functions in a thue-morse chain, *Phys. Rev. B* **46**, 5162 (1992).
- [62] I. Suslov, Localization in one-dimensional incommensurate systems, *Zh. Eksp. Teor. Fiz.* **83**, 1079 (1982).
- [63] T. C. Halsey, M. H. Jensen, L. P. Kadanoff, I. Procaccia, and B. I. Shraiman, Fractal measures and their singularities: The characterization of strange sets, *Phys. Rev. A* **33**, 1141 (1986).
- [64] F. Wegner, Inverse participation ratio in $2+\epsilon$ dimensions, *Z. Phys. B* **36**, 209 (1980).
- [65] R. J. Bell and P. Dean, Atomic vibrations in vitreous silica, *Discuss. Faraday Soc.* **50**, 55 (1970).
- [66] A. Chhabra and R. V. Jensen, Direct determination of the $f(\alpha)$ singularity spectrum, *Phys. Rev. Lett.* **62**, 1327 (1989).
- [67] M. Janssen, Multifractal analysis of broadly-distributed observables at criticality, *Int. J. Mod. Phys. B* **8**, 943 (1994).
- [68] B. Huckestein, Scaling theory of the integer quantum Hall effect, *Rev. Mod. Phys.* **67**, 357 (1995).
- [69] N. Roy and A. Sharma, Fraction of delocalized eigenstates in the long-range Aubry-André-Harper model, *Phys. Rev. B* **103**, 075124 (2021).
- [70] Y. Hashimoto, K. Niizeki, and Y. Okabe, A finite-size scaling analysis of the localization properties of one-dimensional quasiperiodic systems, *J. Phys. A* **25**, 5211 (1992).